Effects of membrane potential on the voltage dependence of motility-related charge in outer hair cells of the guinea-pig

J. Santos-Sacchi, S. Kakehata and S. Takahashi

Sections of Otolaryngology and Neurobiology, Yale University School of Medicine, New Haven, CT 06510, USA

(Received 24 November 1997; accepted after revision 11 March 1998)

1. Isolated outer hair cells (OHCs) from the guinea-pig were whole-cell voltage clamped to study the influence of initial voltage on the voltage dependence of motility-related gating current or, equivalently, on the voltage dependence of membrane capacitance.

2. Prepulse delivery caused changes in the magnitude of motility-related gating currents, which are due predominantly to shifts in the voltage at peak capacitance (V_{pkC_m}). Depolarization shifts V_{pkC_m} in the hyperpolarizing direction, and hyperpolarization does the opposite. The mean shift between −120 and +40 mV prepulse states with long-term holding potentials (> 2 min) at −80 mV was 14·67 ± 0·95 mV ($n = 10$; mean ± S.E.M.).

3. The effect of initial membrane potential is sigmoidal, with a voltage dependence of 23 mV per e-fold change in V_{pkC_m}, and maximum slope within the physiological range of OHC resting potentials. This indicates that the cell is poised to respond maximally to changes in resting potential.

4. The kinetics of prepulse effects are slow compared with motility-related gating current kinetics. High-resolution measurement of membrane capacitance (C_m) using two voltage sinusoids indicates that shifts in V_{pkC_m} induce C_m changes with time courses fitted by two exponentials (τ_0, 0·070 ± 0·003 s; τ_1, 1·28 ± 0·07 s; A_0, 1·54 ± 0·13 pF; A_1, 1·51 ± 0·13 pF; means ± S.E.M.; $n = 22$; step from +50 to −80 mV). Recovery of prepulse effects exhibits a similar time course.

5. Prepulse effects are resistant to intracellular enzymatic digestion, to fast intracellular calcium buffers, and to intracellular pressure. Through modelling, we indicate how the effect may be explained by an intrinsic voltage-induced tension generated by the molecular motors residing in the lateral membrane.

The outer hair cell (OHC) is one of two receptor cell types within the organ of Corti, and plays a critical role in mammalian hearing. The OHC sharpens the passive mechanical vibration of the cochlear partition through a mechanical feedback mechanism (Ruggero, 1992). The basis of this high-frequency feedback mechanism is believed to be the unique voltage-dependent mechanical activity of the cell (Brownell, Bader, Bertrand & de Ribaupierre, 1985; Ashmore, 1987; Santos-Sacchi & Dilger, 1988). This electro-mechanical transduction is mirrored by an electrical signature, a voltage-dependent capacitance or, correspondingly, a gating charge movement (Ashmore, 1989; Santos-Sacchi, 1990, 1991), which may indicate that membrane-bound voltage sensor-motor elements control OHC length (Santos-Sacchi, 1990, 1991, 1993; Ashmore, 1992; Iwasa, 1993). Indeed, estimates of the OHC membrane-bound charge density responsible for the non-linear capacitance (7500 $e^- \mu m^{-2}$; Huang & Santos-Sacchi, 1993) coincide fairly well with estimates of the density of OHC intramembranous particles, the putative sensor-motor elements, observed with electronmicroscopy (6000 μm^{-2}; Forge, 1991). One currently held hypothesis is that these membrane motors control OHC length via membrane areal changes induced by voltage-dependent, two-state conformational changes (Santos-Sacchi, 1993; Iwasa, 1994).

The voltage-dependent mechanical response may be dynamically modulated by a variety of physiologically important factors that can modify the mechanical gain of the cell. One of the most effective means of influencing the motility function is by exerting tension on the plasma membrane (Iwasa, 1993). Reducing membrane tension effectively increases the mechanical gain at the normal resting potential, by shifting the most sensitive region of the motility function along the voltage axis towards the resting potential value (Kakehata & Santos-Sacchi, 1995). Ligand-gated ion channels which can alter the resting membrane potential (Ashmore & Ohmori, 1990; Housley & Ashmore, 1993) may also influence the mechanical gain of the cell by moving the cell operating point, i.e. resting

potential, closer or further away from the most sensitive region of the motility function. Thus, either shifts in resting potential or shifts in the voltage dependence of OHC motility can alter the gain of the cochlear amplifier. We report here that these two mechanisms are not independent. That is, a change in resting potential affects the voltage dependence of OHC capacitance and motility. Furthermore, through modelling, we indicate that the effect can be explained by motor-driven tension on viscoelastic elements within the lateral plasma membrane.

METHODS

OHCs were freshly isolated from the organ of Corti of the guinea-pig cochlea following anaesthetic overdose (halothane inhalant; Halocarbon Labs, NJ, USA) and decapitation (Kakehata & Santos-Sacchi, 1995). The cells were whole-cell voltage clamped at −80 mV (unless otherwise noted) using an Axon 200B amplifier with patch pipettes having initial resistances of 2–3 MΩ, corresponding to tip sizes of 1–2 μm. No series resistance compensation was performed. Residual series resistance (R_s) ranged from 3–7 MΩ. Ionic blocking solutions were used to remove voltage-dependent ionic conductances so that capacitive currents could be analysed in isolation (Santos-Sacchi, 1991; Huang & Santos-Sacchi, 1993). The patch pipette solution contained (mM): 140 CsCl, 2 $MgCl_2$, 10 EGTA and 10 Hepes, pH 7·2 and 300 mosmol l^{-1} (adjusted with dextrose). The external solution contained (mM): 100 NaCl, 20 TEA, 20 CsCl, 2 $CoCl_2$, 1·52 $MgCl_2$, 10 Hepes and 5 dextrose, pH 7·2, 300 mosmol l^{-1}. In some experiments, modifications to the standard solutions were made: pipette solution, replacement of 10 mM EGTA with 10 or 20 mM BAPTA, or inclusion of pronase or trypsin (500 μg ml^{-1}); extracellular solution, inclusion of neomycin (1 mM), or sodium salicylate (5 mM). Drugs were obtained from Sigma, and were selectively applied to individual cells by local perfusion, during simultaneous whole-chamber perfusion with control solution. Experiments were performed at room temperature (21–23 °C).

Three methods were used to analyse OHC motility-related gating charge movement and the corresponding non-linear membrane capacitance. Gating currents were extracted with the $P/-5$ leakage subtraction procedure (Bezanilla & Armstrong, 1977) using a subtraction holding potential of +60 mV. This procedure permits isolation of non-linear capacitive currents by subtracting out the intrinsic linear membrane capacitive currents obtained at a potential where non-linear currents do not contribute significantly. Fits of charge movement were made with a two-state Boltzmann function.

Detailed evaluation of membrane capacitance was made at different potentials by transient analysis of currents induced by a voltage stair-step stimulus (10 mV stair steps from a holding potential of −150 mV to +40 mV). The full stair-step duration was variable and depended upon the time constant of the clamp amplifier; the duration of each individual step was automatically adjusted to 15 times the clamp time constant determined immediately before presentation of the stair-step protocol. This was done to ensure a steady-state current response at each progressive step. Since our clamp time constant was typically less than 0·15 ms, each step was about 2·25 ms in duration. Given twenty, 10 mV incrementing steps in the stair-step, the total duration of the protocol was about 45 ms. The time between prepulse and stair-step was 10 ms and was spent at the prior long-term (> 2 min) holding potential, which was either 0 mV (Fig. 2) or −80 mV (Fig. 3). Thus, a full capacitance function can be obtained within 45 ms with this technique. The capacitance function was fitted to the first derivative of a two-state Boltzmann function relating non-linear charge to membrane voltage (dQ/dV; Santos-Sacchi, 1991; Huang & Santos-Sacchi, 1993),

$$C_m = Q_{max}\frac{ze}{kT}\frac{b}{(1+b)^2} + C_{lin}, \quad (1a)$$

where

$$b = \exp\left(\frac{-ze(V - V_{pkC_m})}{kT}\right), \quad (1b)$$

Q_{max} is the maximum non-linear charge moved, V_{pkC_m} is voltage at peak capacitance or, equivalently, at half-maximal non-linear charge transfer, V_m is membrane potential, z is valency, C_{lin} is linear membrane capacitance, e is electron charge, k is the Boltzmann constant, and T is absolute temperature.

Continuous high-resolution capacitance measures were acquired through admittance (Y) analysis at time resolutions of 5·12 or 2·56 ms, utilizing a two-sine wave voltage-stimulus protocol. The stimulus consisted of the sum of two voltage sine waves (390·625 and 781·25 Hz), each at a magnitude (V) of 10 mV peak. Two (one) full cycles of the low-frequency signal and four (two) full cycles of the high-frequency signal (512 (256) points at 10 μs sampling rate) were continuously delivered every 5·12 (2·56) ms, and the real and imaginary components of the current responses were obtained through Fast Fourier Transform every 5·12 (2·56) ms. The analysis, which was performed in real time and saved to disk, is model dependent; the OHC clamp was modelled as a pipette resistance (R_s) in series with a parallel combination of membrane resistance (R_m) and capacitance (C_m) (Santos-Sacchi, 1993). Given an independent measure of input resistance of such a model and the real and imaginary components of the current response to single sinusoidal stimulation, Pusch & Neher (1988) provide solutions for C_m, R_s and R_m:

$$R_s = (A - b)/(A^2 + B^2 - Ab), \quad (2)$$

$$R_m = (1/b)[(A - b)^2 + B^2]/(A^2 + B^2 - Ab), \quad (3)$$

$$C_m = [1/(\omega B)][(A^2 + B^2 - Ab)^2]/[(A - b)^2 + B^2], \quad (4)$$

where,

$$b = 1/(R_s + R_m) = 1/R_{in},$$
$$Y = I/V,$$
$$A = \mathrm{Re}(Y),$$
$$B = \mathrm{Im}(Y),$$
$$\omega = 2\pi f,$$

and Re is real, Im is imaginary, and f is frequency. Since R_s remains the same at each of the two stimulating frequencies, the input resistance, R_{in}, can be obtained without an independent measure, as is required by the Pusch & Neher technique.

In some experiments, OHCs were collapsed and re-inflated by pipette pressure. Pipette pressure was modified with a syringe connected to the Teflon tubing attached to the patch pipette holder, and was monitored via a T-connector to a pressure monitor (WPI, FL, USA). Voltages were corrected for the effects of residual series resistance. All experiments were video taped. Data collection and analysis were performed with an in-house developed Windows-based whole-cell voltage clamp program, jClamp (www.med.yale.edu/surgery/otolar/santos/jclamp.html), utilizing a Digidata 1200 board (Axon Instruments). Fits were made with the Levenberg–Marquardt least-squares algorithm. Data are presented as means ± standard error of the mean.

RESULTS

The OHC generates gating-like currents when the membrane potential is stepped away from the holding potential (Fig. 1). The decay time constant of the current is very fast (in this example, ~110 μs for the current at voltage offset), and essentially follows the speed of the voltage-clamp stimulus (Santos-Sacchi, 1992; however, see Gale & Ashmore, 1997). Charge movement induced by a step from 0 to −60 mV was increased by prepulsing the OHC to negative voltages. Prepulse effects were clearly evident for durations greater than 30 ms and appeared to plateau at values greater than 1 s (Fig. 1*C*). A single-exponential fit to the charge increase induced by −120 mV prepulses at increasing durations (Fig. 1*C*, inset) gave a time constant of 200 ms.

Figures 2*A* and *B* indicate that voltage prepulse can cause a shift in the voltage dependence of the charge movement or, correspondingly, the capacitance of the cell. In this example, a 1 s prepulse to +40 mV produced a voltage at peak capacitance ($V_{\mathrm{pk}C_{\mathrm{m}}}$) or voltage at half-maximal charge movement (V_{h}) of −76·5 and −83·4 mV, respectively. A 1 s prepulse to −120 mV shifted the values to −56·8 and −56·7 mV. The differences in the magnitude of the fitted shift may have arisen from the inherent difference in prepulse delivery for each data collection protocol. In the case of stair-step analysis, a single prepulse preceded the entire stair-step stimulus, while in the *P*/−5 procedure, a prepulse preceded each step potential. The shift of these functions along the voltage axis was opposite to that of the prepulse direction. Furthermore, the shift in the voltage dependence of OHC capacitance (viz. $\delta V_{\mathrm{pk}C_{\mathrm{m}}}$) was non-linearly related to initial voltage. Figure 2*C* shows that the relation was sigmoidal and, significantly, the greatest sensitivity to prepulse was within the physiological voltage range. OHCs normally have resting potentials near −70 mV (Dallos, Santos-Sacchi & Flock, 1982). The maximum mean shift due to a 1 s prepulse was 14·8 mV, with a voltage slope factor of 22·2 mV, and a mid-point voltage of −54·4 mV ($n = 4$).

The effects of prepulse were reversible on the same time scale as onset. Figure 2*D* depicts the mean ($n = 22$) recovery from a 1 s prepulse to 50 mV. After a 1 s recovery at −150 mV, $V_{\mathrm{pk}C_{\mathrm{m}}}$ has nearly recovered to steady state from the prepulse-induced shift. A single-exponential fit to $V_{\mathrm{pk}C_{\mathrm{m}}}$ (Fig. 2*D*, inset) gave a time constant of 330 ms. Under these conditions, the mean $V_{\mathrm{pk}C_{\mathrm{m}}}$ shift was about 10 mV.

The data of Figs 1 and 2 were obtained with the cells held at a long-term holding potential of 0 mV, because whole-cell recording stability was better at this potential; in order to demonstrate the physiological relevance of the observed prepulse phenomenon, additional experiments were conducted at long-term holding potentials of −80 mV prior to the evaluation of prepulse effects. Figure 3 illustrates that the phenomenon remains qualitatively and quantitatively the same under such conditions. The mean shift between −120 mV and +40 mV prepulse states with long-term holding potentials (> 2 min) at −80 mV was 14·67 ± 0·95 mV ($n = 10$).

The time course of prepulse effects is slow compared with the gating current time constants. In order to confirm the stair-step and *P*/*N* kinetic data, we utilized another technique to garner high-resolution information on the time course of prepulse effects. Since the shift in $V_{\mathrm{pk}C_{\mathrm{m}}}$ will necessarily cause the capacitance measured at a fixed potential to change, the time course of the capacitance change can be used to study prepulse effect kinetics. This is illustrated in Fig. 4, where OHC capacitance was monitored as the cell was stepped from a holding potential of +50 mV

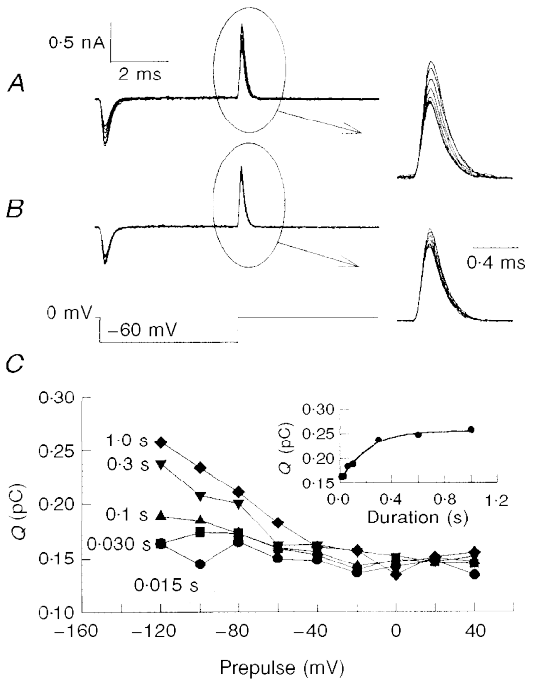

Figure 1. Motility-related charge movement is affected by initial voltage conditions

At a fixed membrane potential, an increase in charge is induced by a negative prepulse. The charge increase is due to the shift in the voltage dependence of charge movement, and the response is time dependent. An OHC was stepped to −60 mV from a holding potential of 0 mV. The command which generated each current trace was preceded by a prepulse of either 1 s (*A*) or 60 ms (*B*), with a magnitude ranging from −120 to +40 mV (20 mV increments). Leakage subtraction (*P*/−5; subtraction hold, 60 mV) revealed gating-like currents associated with OHC motility. As the length of prepulse increased, charge increased. *C*, under these conditions, prepulse effects were clearly present at potentials more negative than −50 mV and at durations greater than 30 ms. Inset shows time course of charge increase induced by prepulse to −120 mV. Fit indicates a single-exponential time constant of 0·2 s.

to −89 mV for 4 s. At the onset, C_m was about 39·8 pF, but decreased during the maintained voltage step to about 35·5 pF (Fig. 4*B*). The time course of this decrease was composed of fast and slow components, which was well fitted by a double exponential (t_0, 0·058 s; t_1, 1·34 s; A_0, 2·2 pF; A_1, 1·48 pF). (It might be expected that the time course would deviate somewhat from a true double exponential, even if the underlying mechanism followed a double-exponential time course, since the change in C_m is not linear, but follows the bell-shaped capacitance function.) The change in C_m was accounted for by a shift in V_{pkC_m} of about +25 mV. This was determined from responses to 25 ms voltage ramps delivered during the course of a maintained voltage step (Fig. 4*A*; arrows indicate ramp presentations). V_{pkC_m}, determined by fits of the resultant capacitance functions, corresponded in time to the relaxation in membrane capacitance (Fig. 4*B*). All cells studied with this high-resolution C_m measurement technique showed a double-exponential time course (τ_0, 0·070 ± 0·003 s; τ_1, 1·28 ± 0·07 s; A_0, 1·54 ± 0·13 pF; A_1, 1·51 ± 0·13 pF; $n = 22$; nominal step from +50 to −80 mV). In order to show that the time course of C_m change is not due to recovery from membrane breakdown at very depolarized potentials, we measured more physiological membrane potential perturbations. Voltage steps from −80 to −40 mV, where membrane stability is unquestionable, produced changes in C_m with similar time courses. Figure 4*C* presents such an example.

The apparent difference in the time course observed with standard transient analysis techniques used in Figs 2 and 3 and the admittance measuring technique is explained by the higher time resolution and measurement density afforded by the latter method. A single-exponential fit to double-exponential data obtained with the admittance method also generates time constants in the tenths of seconds range when the extent is limited to 1 s, and few data points are sampled. It should also be noted that the duration of the stair-step protocol, typically around 50 ms, is close to τ_0, and, as such, some V_{pkC_m} shift may have accumulated during that ramped measurement.

The actual direction and magnitude of C_m change during a shift in V_{pkC_m} depended on the initial holding potential and the step potential *vis-à-vis* the initial V_{pkC_m}. This is illustrated in Fig. 5*A* where the OHC membrane potential was stepped through V_{pkC_m} in 10 mV increments. Steps in potential induced essentially instantaneous jumps in C_m followed by slower changes. Small voltage steps from the initial holding level produced small time-dependent changes

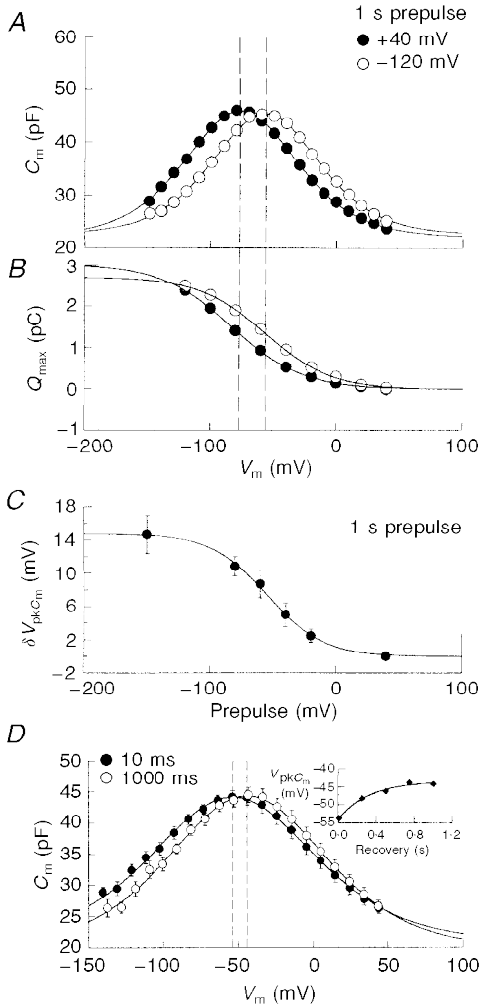

Figure 2. Voltage prepulse causes a shift in the voltage dependence of charge movement and non-linear capacitance

Long-term holding potential was 0 mV. Voltage-dependent capacitance was evaluated with the stair-step technique (*A*), and corresponding gating charge movement was evaluated with the *P*/−5 technique at a subtraction holding potential of +60 mV (*B*). With either technique, voltage dependence was evidenced by a shift in the positive direction for negative prepulses (1 s duration). The shift is about 20 mV for a 40 mV prepulse (V_{pkC_m} is indicated by the dashed lines). Continuous line fit in *A* for −120 mV prepulse: V_{pkC_m}, −56·8 mV; z, 0·9; Q_{max}, 2·6 pC; C_{lin}, 22·5 pF; peak C_m ($C_{m,pk}$), 45·4 pF. For +40 mV prepulse: V_{pkC_m}, −76·5 mV; z, 0·86; Q_{max}, 2·86 pC; C_{lin}, 22·0 pF, $C_{m,pk}$, 45·9 pF. Continuous line fit in *B* for −120 mV prepulse: V_h, −56·7 mV, z, 0·96; Q_{max}, 2·7 pC. For +40 mV prepulse: V_h, −83·4 mV; z, 0·90; Q_{max}, 3·0 pC. *C*, the shift in voltage dependence is sigmoidal. The plot illustrates for 4 cells the mean (± S.E.M.) shift in the voltage at peak capacitance, obtained with the stair-step technique. The sigmoidal continuous line fit ($\delta V_{pkC_m} = a/[1 + \exp((V_{prepulse} - V_h)/b)]$) indicates a maximum mean shift, a, of 14·8 mV, a slope factor, b, of 22·2 mV, and a mid-point voltage, V_h, of −54·4 mV. Data are normalized to +40 mV response. *D*, recovery from prepulse effects has a similar time course to onset. Mean (± S.E.M.) from 22 cells. V_{pkC_m} was evaluated with the stair-step protocol from a holding potential of −150 mV. A 1 s prepulse to 50 mV preceded recovery durations of 10, 250, 500, 750 and 1000 ms at −150 mV. Only the 10 ms and 1000 ms recovery functions are shown. Inset shows time course of V_{pkC_m} recovery. Fit indicates a single-exponential time constant of 0·33 s. Recovery from prepulse appears nearly complete at 1 s. Continuous line fit for 10 ms recovery: V_{pkC_m}, −53·7 mV; z, 0·7; Q_{max}, 3·39; C_{lin}, 20·9 pF. Continuous line fit for 1000 ms recovery: V_{pkC_m}, −44·2 mV; z, 0·73; Q_{max}, 3·45 pC; C_{lin}, 19·8 pF. Parallel dashed lines indicate the V_{pkC_m} of each function.

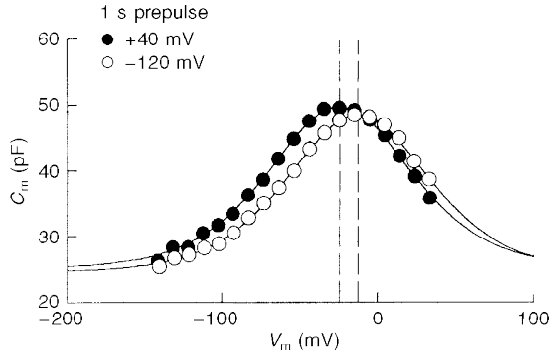

Figure 3. Prepulse-induced shifts occur at physiological holding potentials

Prepulse-induced shift of capacitance function after an OHC was held at a long-term holding potential of −79 mV. As with depolarized long-term holding potentials, prepulses from physiological holding potentials caused a shift in the positive direction for negative prepulses (1 s duration). The shift in this case is 11·8 mV for a 40 mV prepulse. Continuous line fit for −120 mV prepulse: V_{pkC_m}, −12·5 mV; z, 0·84; Q_{max}, 2·9 pC; C_{lin}, 24·7 pF; $C_{m,pk}$, 48·5 pF. For +40 mV prepulse: V_{pkC_m} −24·3 mV; z, 0·84; Q_{max}, 3·0 pC; C_{lin}, 25·2 pF, $C_{m,pk}$, 49·8 pF.

in C_m because the magnitude of V_{pkC_m} shift was small. Progressively larger voltage steps produced larger V_{pkC_m} shifts and, thus, larger changes in C_m at each fixed step potential. The direction of capacitance change was increasing for voltage steps positive to V_{pkC_m}, and decreasing for voltage steps negative to V_{pkC_m}. Also note for this protocol that C_m at the holding potential accumulated somewhat over time because full C_m relaxation was not reached during the interstep recovery period. Figure 5*B* shows the effect of voltage-step duration on the non-linear capacitance function. Determination of C_m at zero time (5 ms; the initial data point measured during a voltage step is contaminated by the transient response) or after 1 s provided differing functions, with the 1 s determination showing a relative compression of the function in the depolarizing direction; indeed, C_m overlap occurred at very depolarized levels. This is expected since the magnitude of prepulse effect is a function of step potential.

There are several possible mechanisms which may account for the observed prepulse effects, including intracellular pressure change. OHC voltage-dependent motility occurs under a constant cell volume constraint (Santos-Sacchi, 1993; Dallos, Hallworth & Evans, 1993). Thus, during whole-cell voltage stimulation, intracellular pressure may change, despite continuity with pipette volume. Since modification of intracellular pressure is known to shift V_{pkC_m} via tension applied to the plasma membrane (Iwasa, 1993; Gale & Ashmore, 1994; Kakehata & Santos-Sacchi, 1995), it is of interest to determine whether prepulse effects are simply related to a motility-induced intracellular pressure change. Figure 6*A* illustrates that when OHCs ($n = 6$) were collapsed with negative pipette pressure, causing a limiting negative shift in V_{pkC_m} (Kakehata & Santos-Sacchi, 1995), prepulse effects were still observed. Collapsed OHCs cannot generate an intracellular pressure change (nor the consequent pressure-induced membrane tension) since the usual voltage-

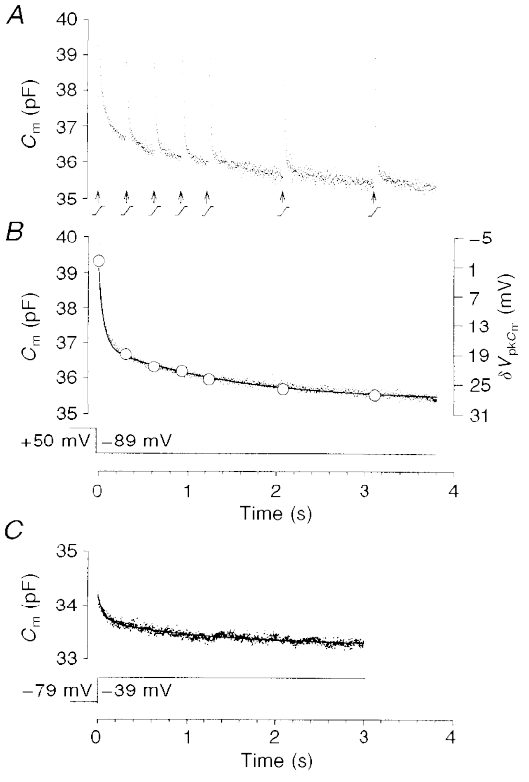

Figure 4. The time course of prepulse effects has a fast and a slow component

A, an OHC was stepped to −89 mV from a holding potential of +50 mV, and the C_m at the new step potential was monitored every 2·5 ms using the admittance technique (see Methods). At the time points indicated, voltage ramps (25 ms in duration) were delivered in order to determine V_{pkC_m} from the voltage-capacitance function. In *B*, the step stimulus was delivered without ramps, and the continuous line (which is difficult to see, since it is obscured by the many data points) is a double-exponential fit to the resultant capacitance data (t_0, 0·058 s; t_1, 1·34 s; A_0, 2·2 pF; A_1, 1·48 pF). The close correspondence of the overlying open symbols, which denote the change in V_{pkC_m} relative to the first ramp measurement (i.e. δV_{pkC_m}), indicates that the shift of the OHC capacitance function along the voltage axis accounts for the relaxation of capacitance during step potentials. *C*, a voltage step from a long-term holding potential (> 2 min) of −79 mV to −39 mV, induces a change in C_m over a similar time course to that in 4*B*. The fitted line (t_0, 0·067 s; t_1, 1·18 s; A_0, 0·46 pF; A_1, 0·44 pF) is obscured by the data points.

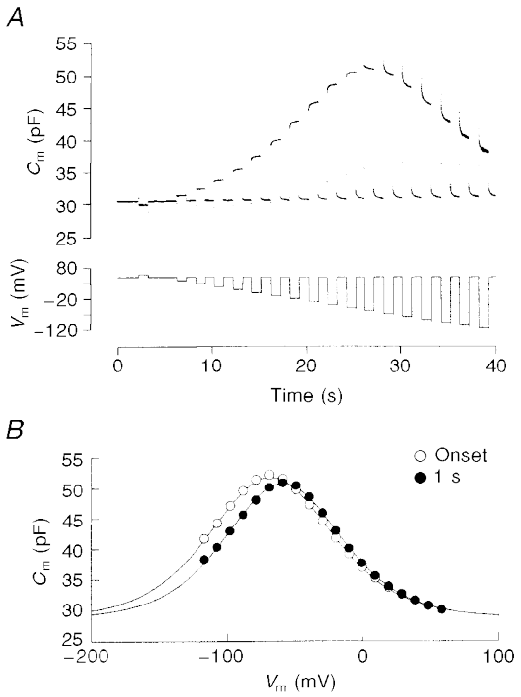

Figure 5. The direction and magnitude of C_m change depends on initial holding potential and step potential relative to V_{pkC_m}

A, an OHC was stepped (−10 mV increments) from a holding potential of +48 mV through V_{pkC_m}. Step durations were 1 s, with equal recovery intervals at the holding potential. A total of 40 s of data were collected at 5 ms resolution. The top panel shows C_m measured with the admittance technique. The bottom panel shows the DC voltage stimulus, corrected for residual series resistance. Note that steps to voltages more depolarized than V_{pkC_m} induce C_m changes which increase over time, while steps to potentials more hyperpolarized than V_{pkC_m} induce C_m changes which decrease over time. The magnitude of C_m change corresponds to step size. *B*, the C_m functions derived from the measurements at onset (5 ms point; the initial data point measured by Fast Fourier Transform during a voltage step is invalid since it is contaminated by the transient response – these aberrant points are visible at the transitions between voltage steps) or 1000 ms are plotted, along with fitted functions. The plots indicate differences in the instantaneous and steady-state C_m functions; notably a shift and compression in the steady-state function in the depolarizing direction. Continuous line fits for onset: Q_{max}, 2·81 pC; z, 0·85; C_{lin}, 28·7 pF; V_{pkC_m}, −68 mV. For steady-state: Q_{max}, 2·54 pC; z, 0·9; C_{lin}, 28·7 pF; V_{pkC_m}, −58·7 mV.

dependent whole-cell mechanical response (but not gating current) is abolished. Prepulse-induced voltage shifts merely superimposed upon the negative pressure-induced steady-state voltage shift. These data suggest that voltage-induced motility induces little or no intracellular pressure changes, in line with modelling efforts (Tolomeo & Steele, 1995).

Other possible prepulse mechanisms might involve intracellular Ca^{2+} increases, and cytoskeletal–motor interactions. These can be excluded since we have found no alterations of prepulse effects upon using the fast Ca^{2+} chelator BAPTA (10 mM ($n = 4$) or 20 mM ($n = 4$)) intracellularly, or after intracellular digestion with pronase ($n = 5$) or trypsin

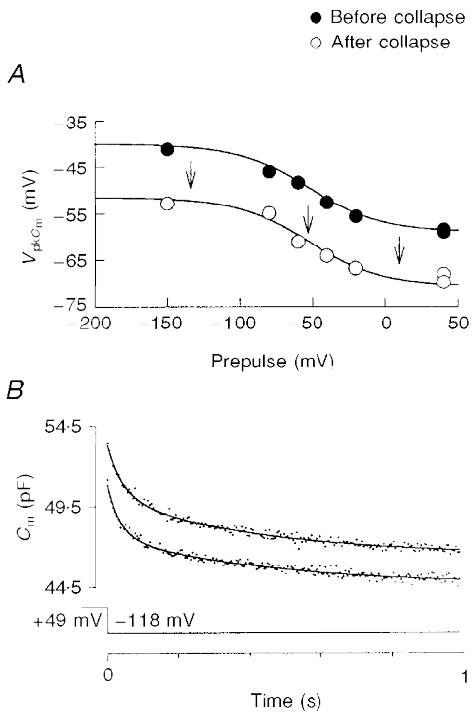

Figure 6. The mechanism responsible for prepulse effects appears intrinsic to the lateral membrane

A, intracellular pressure does not alter prepulse effects. Before (●) and after (○) collapse of OHC by reduction of intracellular pressure via patch pipette. Note the parallel negative shift in V_{pkC_m} with negative pressure. Prepulse at each potential was 1 s in duration. The sigmoidal lines were generated with the electro-mechanical model described in the Discussion. Parameter values are the same as set out in the Discussion, except that for the continuous line corresponding to data before collapse: μ_1, 4 mN m^{-1}; η_1, 0·24 mN s m^{-1}; μ_2, 4 mN m^{-1}; and η_2, 4·8 mN s m^{-1}. The continuous line corresponding to data after cell collapse was generated with the same parameters except that a constant of 1 kTorr was subtracted from the mechanical energy, E_m, to account for the resultant decrease in membrane tension (see Discussion for model details). *B*, C_m measurements made before (zero time after whole-cell configuration, bottom trace) and after (10 min after whole-cell configuration, top trace) intracellular pronase treatment (500 μg ml^{-1}, delivered via the patch pipette). After 10 min, the cell had lost its cylindrical shape and formed a sphere. The cell was held at +49 mV and stepped to −118 mV for 1 s. In each case the onset C_m relaxed with a double-exponential time course. The difference in absolute magnitude (DC) is due to a steady-state shift in V_{pkC_m}, from −90·7 to −97·6 mV, possibly induced by osmotic effects or a release in tension on the membrane after cytoskeletal disruption. Such shifts during intracellular enzymatic treatments have been noted previously (Huang & Santos-Sacchi, 1994). The relaxations are quite similar, indicating that the treatment had little effect on the molecular structures responsible for voltage-induced V_{pkC_m} shift. The continuous lines indicate the sum of two exponentials – zero time: τ_0, 0·034 s; τ_1, 0·447 s; 10 min: τ_0, 0·042 s; τ_1, 0·417 s.

($n = 4$; 500 mg ml^{-1}). Intracellular proteolytic treatment has been shown to abolish normal OHC cyto-architecture by disrupting the cortical cytoskeleton and subsurface cisternae (Huang & Santos-Sacchi, 1994). An example of the negligible effect of intracellular pronase treatment on voltage-dependent V_{pkC_m} shift is provided in Fig. 6*B*. Another indication that the V_{pkC_m} shift was unrelated to intracellular structures is the poor correlation between the fitted C_m exponential parameters and precise estimates of cell length, viz. linear capacitance ($r^2$of τ_0 *vs.* C_{lin}, 0·23; r^2 of τ_1 *vs.* C_{lin}, 0·15; r^2 of A_0 *vs.* C_{lin}, 0·004; r^2 of A_1 *vs.* C_{lin}, 0·033; $n = 22$; step from +50 mV to −80 mV). It should be noted that the pronase and trypsin experiments also exclude a host of biochemical processes which would rely on enzymes susceptible to proteolytic destruction, for example protein kinases. Other treatments which did not interfere with prepulse effects were salicylate (sub-maximal dose, 5 mM; $n = 5$), and neomycin (1 mM; $n = 3$).

DISCUSSION

The OHC possesses a voltage-dependent capacitance or gating charge movement with a V_{pkC_m} or mid-point voltage, V_h, that is variable (Santos-Sacchi, Huang & Kakehata, 1994). The present data indicate that one of the factors contributing to this variability is a dependence on initial voltage conditions. More importantly, since motility-related gating charge characteristics are known to mirror characteristics of the mechanical activity of the OHC (Ashmore, 1989, 1992; Santos-Sacchi, 1991, 1992; Kakehata & Santos-Sacchi, 1995), the present experiments demonstrate a link between the two factors, membrane potential and V_{pkC_m}, that control the gain of OHC motility.

Some superficial characteristics of prepulse effects on OHC motility-related gating currents are reminiscent of the Cole–Moore effect on K^+ channel gating currents (Cole & Moore, 1960; Stefani, Toro, Perozo & Bezanilla, 1994); however, no shift in voltage dependence is associated with the Cole–Moore effect. On the other hand, a shift in voltage dependence is responsible for depolarization-induced fast (complete within 50 ms) and slow (occurring over seconds to minutes) inactivation of Na^+ channel gating (Bezanilla, Taylor & Fernandez, 1982). Inactivation of Na^+ channels is characterized by charge immobilization (Armstrong & Bezanilla, 1977; Bezanilla & Armstrong, 1977). We had previously noted an absence of OHC charge immobilization on very short time scales (within a window of 26 ms; Fig. 9 in Santos-Sacchi, 1991), where Na^+ channel gating charge immobilization is clearly observed. Given the present results, this is understandable since in the OHC the fast prepulse effect has a mean time constant of 70 ms; additionally, since the voltage dependence of OHC charge movement is significantly less steep than Na^+ channel gating charge movement, a given shift in voltage dependencies will present a smaller charge immobilization for the OHC. In preliminary experiments, an extended observation window permits the observation of charge immobilization in the OHC, with a time course similar to the capacitance data. To a limited extent, then, Na^+ channel gating behaviour is comparable to that of the OHC lateral membrane motor. Simple kinetic schemes to account for prepulse effects on the Na^+ channel were discussed by Bezanilla *et al.* (1982), and may possibly apply to the OHC. These abstract schemes do not, however, provide insight into the physical correlates of prepulse effects in the OHC.

The present data suggest that voltage prepulse appears to work directly on the lateral membrane and/or the embedded molecular motors, and not via extrinsic tension delivered by intracellular pressure or delivered by some other means, e.g. Ca^{2+}-dependent cytoskeletal interactions or enzyme-based second messengers. While an extrinsic source of tension can probably be ruled out, an intrinsic source of tension can be envisioned. In this regard, it is notable that the magnitude of voltage prepulse effects presents characteristics similar to those of OHC motility itself. Namely, the sigmoidal voltage dependence is similar between the two. It is, therefore, conceivable that the activity (conformational changes) of the molecular motors themselves produces a force within the lateral membrane which dynamically modifies V_{pkC_m}. Thus, while the electrical energy supplied by the membrane potential will drive lateral molecular motors into a preferred state, leading to an overall change in membrane area, the force induced by this strain within the viscoelastic membrane will influence the state of adjacent motors, but will decay over time. In order to account for the kinetics of V_{pkC_m} shift, the induced membrane tension must dissipate following the time course observed in the OHC C_m measurements (Figs 4 and 5). Iwasa (1994) evaluated the effects of an externally applied tension on the OHC membrane by redefining eqn (1) to include an additional energy term (E_m) in the description of OHC C_m:

$$b = \exp\left(\frac{-ze(V - V_{pkC_m}) + E_m}{kT}\right), \quad (5)$$

where E_m, the mechanical energy per motor unit, was calculated from the product of a, the unit areal change in the lateral membrane motor, and T_m, the mean membrane tension in the axial and circumferential directions, determined from the law of Laplace. From Iwasa (Fig. 4, 1993) and Kakehata & Santos-Sacchi (Fig. 4, 1995), it is known that 1 kPa intracellular pressure induces an OHC longitudinal strain ($\Delta L/L$) of 0·07. Such a longitudinal strain corresponds to a shift in V_{pkCm} of 22·5 mV (Kakehata & Santos-Sacchi, 1995), and can be accounted for by an induced membrane mechanical energy of 1·2 kT according to eqns (1*a*) and (5).

We model E_m as being additionally voltage and time dependent. The voltage-dependent characteristics match those of OHC motility, and the time-dependent characteristics accord with the time constants of OHC C_m measurements. Depolarization, which drives the motors into

a compact state, induces tension in the membrane. The electro-mechanical model is implemented as follows.

The patch-clamped OHC is modelled electrically as an electrode resistance (R_s) in series with a parallel combination of a membrane resistance (R_m), linear capacitance (C_{lin}) and voltage-dependent capacitance (C_v) as defined above (see Santos-Sacchi, 1993, for details). The electrical model parameters are: R_s, 5 MΩ; R_m, 100 MΩ; C_{lin}, 29 pF; Q_{max}, 2·3 pC; V_{pkC_m}, −50 mV; and z, 1. Voltage-dependent OHC contraction, δL, is described by a two-state Boltzmann function (Santos-Sacchi, 1991):

$$\delta L = \frac{\delta L_{max}}{1 + \exp\left(\frac{-ze(V - V_{pkC_m}) + E_m}{kT}\right)}, \quad (6)$$

now including the additional mechanical energy term E_m, which is derived from the deformation-induced membrane force (F).

$$E_m = F_m \times \delta d_m, \quad (7)$$

$$F_m = F/N_{cir}, \quad (8)$$

where F_m is the force per motor unit, determined by dividing whole-cell membrane force (F) by N_{cir}, the number of parallel motors along the circumferential dimension of the OHC. δd_m is the diameter change of the lateral membrane motor.

The OHC lateral membrane is modelled as a parallel combination of Maxwell (series combination of spring and dash-pot) elements (standard 4-parameter Maxwell model; Tschoegl, 1989) (inset in Fig. 7*A*). The equations describing the mechanical model are:

$$\frac{dx}{dt} = \frac{\dot{F}_1}{\mu_1} + \frac{F_1}{\eta_1} = \frac{\dot{F}_2}{\mu_2} + \frac{F_2}{\eta_2}, \quad (9)$$

$$F = F_1 + F_2, \quad (10)$$

where the dot, e.g. in $\dot{F}_1$, indicates differentiation with respect to time, μ_1 and μ_2 are the spring stiffness coefficients, and η_1 and η_2 are the dash-pot coefficients of viscosity.

The force induced by step deformation is a decaying double-exponential function of time:

$$F = x[\mu_1 \exp(-t/\tau_1) + \mu_2 \exp(-t/\tau_2)], \quad (11)$$

where:

$$\tau_1 = \eta_1/\mu_1,$$

$$\tau_2 = \eta_2/\mu_2,$$

$$x = 0,\ t \leqslant 0,$$

$$x = 1,\ t > 0,$$

and the deformation of the model, x, is obtained from the motility function $\delta L(V)$. Maximum contraction, δL_{max}, is set at 3 μm (Santos-Sacchi & Dilger, 1988). The parameter values of the mechanical elements are chosen to produce maximal instantaneous voltage-dependent mechanical energy (E_m) of 1·2 kT, and to provide a double-exponential time course for the relaxation of that energy which matches the time course empirically determined in Fig. 5. The mechanical parameter values which satisfy these conditions are: μ_1, 5·8 mN m^{-1}; η_1, 0·35 mN s m^{-1}; μ_2, 4·2 mN m^{-1}; and η_2, 5 mN s m^{-1}. δd_m is set to 0·5 nm and N_{cir} is 3000 (Santos-Sacchi, 1993). Notably, our model is of the plasma membrane, since contributions by intracellular structures have been dismissed. In this regard, our model differs from classical treatments of the red cell membrane (e.g. Chien, Sinu, Skalak, Usami & Tozeren, 1978) and a recent treatment of OHC viscoelastic behaviour (see below; Ehrenstein & Iwasa, 1996), since, in those analyses, cytoskeletal element contributions were not ruled out. The model was evaluated with the software package Simulink (Mathworks, MA, USA) or hard-coded in C. Maximum force (F) generated with the model is about 30 nN. This compares favourably with the force determined from whole-cell stiffness measurements (10 mN m^{-1} × 3 μm = 30 nN; Hallworth, 1996; Iwasa & Adachi, 1997), or voltage-dependent force estimates (0·1 nN mV^{-1} × 200 mV = 20 nN; Hallworth, 1996; Iwasa & Adachi, 1997). The stiffness coefficients for the membrane spring components are also in good agreement with the OHC membrane stiffness estimate (1 mN m^{-1}) of Tolomeo, Steele & Holley (1996); the values are greater than red blood cell plasma membrane stiffness (10 μN m^{-1}; Skalak, Tozeren, Zarda & Chein, 1973).

Figure 7 illustrates the results obtained from the model when it is stimulated with the same voltage protocol used in Fig. 5. The voltage-dependent mechanical energy which develops is shown in the middle panel of Fig. 7*A*, and at large voltage steps approaches instantaneous values of 1 kT, followed by relaxations towards zero. The model was also used to account for the data in Fig. 6*A*, indicating its usefulness in describing prepulse effects. The similarity between the capacitance of the model and OHC indicates that tension developed by the voltage-driven molecular motors residing within the lateral membrane can account for the biophysical data.

Because of the correspondence between OHC capacitance and motility, the length of the OHC is expected to mirror the intrinsic tension-dependent changes in C_m. However, the physiological significance of the link between membrane potential and the voltage dependence of OHC capacitance and motility is dependent on the magnitude and time course of the phenomenon. The magnitude of V_{pkC_m} shift is maximal in the physiological voltage range, showing a voltage dependence of about 22 mV per e-fold change in V_{pkC_m}. A step in membrane potential will produce not only a very rapid change in cell length, but, in addition, a slow length change as V_{pkC_m} shifts. Given the model parameters used above, the ratio of slow length change to rapid length change following a voltage step from the resting potential of −70 mV is a bell-shaped function of step voltage, with a maximum of about 0·2 at a voltage near the resting

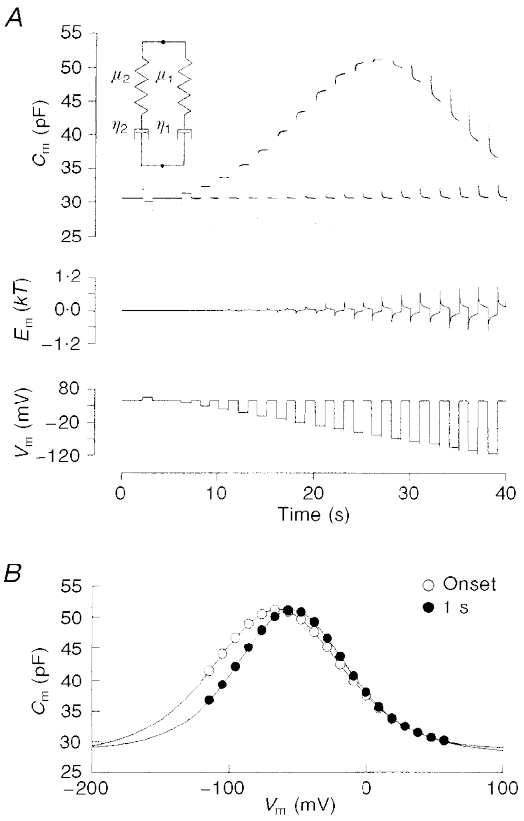

Figure 7. Model results incorporating a voltage-induced mechanical energy within the plasma membrane

A, the top panel shows the whole-cell capacitance induced by the voltage stimulus in the bottom panel. Same voltage protocol as used in Fig. 5. The middle panel shows the generated mechanical energy, E_m. Model C_m results are quite similar to the OHC C_m data of Fig. 5. Inset, viscoelastic model of membrane, consisting of a parallel combination of two Maxwell elements (series combination of spring and dash-pot). The symbols μ_1 and μ_2 indicate the spring stiffness coefficients, and the symbols η_1 and η_2 indicate the dash-pot coefficients of viscosity. *B*, onset (5 ms) and steady-state (1 s) C_m function as in Fig. 5*B*. Continuous line fits for onset: Q_{max}, 2·94 pC; z, 0·81; C_{lin}, 28·1 pF; V_{pkC_m}, −65·1 mV. For steady state: Q_{max}, 2·42 pC; z, 0·95; C_{lin}, 28·7 pF; V_{pkC_m}, −54·8 mV.

potential. An example of the mechanical response of the model is shown in Fig. 8. This is a significant component of the length change, and such a slow length change is observable in records of OHC mechanical responses obtained under whole-cell voltage clamp (Ashmore, 1987; Santos-Sacchi, 1990, 1992).

The physical basis of the time course of V_{pkC_m} shift observed here probably derives from viscoelastic elements within the motor itself and/or within the lipid bilayer. Alterations in the mechanical properties of these structures may, therefore, control the time course of the phenomenon. Nevertheless, the double-exponential time course indicates that the mechanism may only be significant at frequencies below about 3 Hz. Even correcting for temperature effects (e.g. Q_{10} for OHC gating charge kinetics is 1·5; Santos-Sacchi, 1990) will not significantly increase the frequency response. However, such slow effects may be utilized by the OHC medial efferent system. The effects of the medial efferent system on the peripheral auditory system encompass the time scales reported here (Sridhar, Liberman, Brown & Sewell, 1995). It is also to be expected that pathological states which cause membrane potential alterations in the OHC, e.g. acoustic overexposure (Cody & Russell, 1985), may evoke V_{pkC_m} shifts with attendant changes in the gain of OHC motility. Since, normally, V_{pkC_m} is more depolarized than the OHC resting membrane potential (Dallos *et al.* 1982; Santos-Sacchi, 1991; Ashmore, 1992; Kakehata & Santos-Sacchi, 1995), a depolarizing shift in resting potential augmented by a hyperpolarizing shift in the motility function should increase mechanical gain, but reduce motor-generated non-linearities; namely, DC and harmonic mechanical components (Santos-Sacchi, 1993). In the peripheral auditory system, where non-linearities are the hallmark of normal activity, such interference with motility-based non-linearities may be significant.

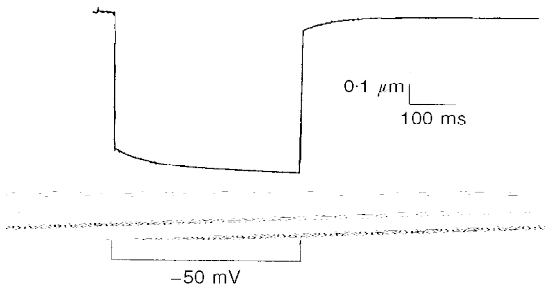

Figure 8. Predicted mechanical responses of the OHC to voltage steps

Model results indicating the slow DC component attributable to motor-induced membrane tension. Step voltage from −70 mV to −50 mV.

Interestingly, Ehrenstein & Iwasa (1996) have observed external, osmotically induced viscoelastic behaviour in the intact OHC with a single time constant of about 40 s. Within this time scale, tension induced by steady-state membrane strain relaxes exponentially. This very slow time course may suggest that the underlying mechanical elements responsible for their observed viscoelastic behaviour are distinct from those responsible for the $V_{\mathrm{pkC_m}}$ shifts observed here. However, it should be noted that the apparent viscosity of a medium may depend upon rate, duration and magnitude of deformation (see Hochmuth, 1993). For example, Chien *et al.* (1978) found that an increase in duration of erythrocyte deformation from 2 to 20 s, caused an increase in the time constant of recovery from about 110 to 260 ms. In this regard, the fast rate and small magnitude of deformation induced by membrane voltage markedly differ from those of the osmotic treatments of Ehrenstein & Iwasa (1996).

Finally, it is noted that the $V_{\mathrm{pkC_m}}$ shift which is induced by voltage-dependent motor activity underlies the existence of both an instantaneous and a steady-state electromechanical transduction function, as exemplified through capacitance measurements (Fig. 5). This is somewhat analogous to the instantaneous and steady-state stereociliar mechano-electrical transducer functions which derive from displacement-induced adaptation (Shepherd & Corey, 1994). In each case, a time-dependent relaxation in a tension produced by the appropriate physiological stimulus on a membrane component (stereociliar channel or OHC motor) will effectively result in a repositioning of the cell operating point along the corresponding transduction function.

Armstrong, C. M. & Bezanilla, F. (1977). Inactivation of the sodium channel. II. Gating current experiments. *Journal of General Physiology* **70**, 567–590.

Ashmore, J. F. (1987). A fast motile response in guinea-pig outer hair cells: the cellular basis of the cochlear amplifier. *Journal of Physiology* **338**, 323–347.

Ashmore, J. F. (1989). Transducer motor coupling in cochlear outer hair cells. In *Mechanics of Hearing*, ed. Kemp, D. & Wilson, J. P., pp. 107–113. Plenum Press, New York.

Ashmore, J. F. (1992). Mammalian hearing and the cellular mechanism of the cochlear amplifier. In *Sensory Transduction*, ed. Corey, D. P. & Roper, S. D., pp. 395–412. Rockefeller University Press, NY, USA.

Ashmore, J. F. & Ohmori, H. (1990). Control of intracellular calcium by ATP in isolated OHCs of the guinea-pig cochlea. *Journal of Physiology* **428**, 109–131.

Bezanilla, F. & Armstrong, C. M. (1977). Inactivation of the sodium channel. I. Sodium current experiments. *Journal of General Physiology* **70**, 549–566.

Bezanilla, F., Taylor, R. E. & Fernandez, J. M. (1982). Distribution and kinetics of membrane dielectric polarization. I. Long-term inactivation of gating currents. *Journal of General Physiology* **79**, 21–40.

Brownell, W. E., Bader, C. R., Bertrand, D. & de Ribaupierre, Y. (1985). Evoked mechanical responses of isolated cochlear outer hair cells. *Science* **227**, 194–196.

Chien, S., Sung, K. L., Skalak, R., Usami, S., & Tozeren, A. (1978). Theoretical and experimental studies on viscoelastic properties of erythrocyte membrane. *Biophysical Journal* **24**, 463–487.

Cody, A. R. & Russell, I. J. (1985). Outer hair cells in the mammalian cochlea and noise-induced hearing loss. *Nature* **315**, 662–665.

Cole, K. S. & Moore, J. W. (1960). Potassium ion current in the squid giant axon: dynamic characteristics. *Biophysical Journal* **1**, 161–202.

Dallos, P., Hallworth, R. & Evans, B. (1993). Theory of electrically driven shape changes of cochlear outer hair cells. *Journal of Neurophysiology* **70**, 299–322.

Dallos, P., Santos-Sacchi, J. & Flock, A. (1982). Intracellular recordings from outer hair cells. *Science* **218**, 582–584.

Ehrenstein, D. & Iwasa, K. H. (1996). Viscoelastic relaxation in the membrane of the auditory outer hair cell. *Biophysical Journal* **71**, 1087–1094.

Forge, A. (1991). Structural features of the lateral walls in mammalian cochlear outer hair cells. *Cell Tissue Research* **265**, 473–483.

Gale, J. E. & Ashmore, J. F. (1994). Charge displacement induced by rapid stretch in the basolateral membrane of the guinea pig OHC. *Proceedings of the Royal Society of London* B **255**, 243–249.

Gale, J. E. & Ashmore, J. F. (1997). An intrinsic frequency limit to the cochlear amplifier. *Nature* **389**, 63–66.

Hallworth, R. (1995). Passive compliance and active force generation in the guinea pig outer hair cell. *Journal of Neurophysiology* **74**, 2319–2328.

Hochmuth, R. M. (1993). Measuring the mechanical properties of individual human blood cells. *Journal of Biomechanical Engineering* **115**, 515–519.

Housley, G. D. & Ashmore, J. F. (1993). Direct measurement of the action of ACh on isolated OHCs of the guinea pig cochlea. *Proceedings of the Royal Society of London* B **244**, 161–167.

Huang, G.-J. & Santos-Sacchi, J. (1993). Mapping the distribution of the outer hair cell motility voltage sensor by electrical amputation. *Biophysical Journal* **65**, 2228–2236.

Huang, G.-J. & Santos-Sacchi, J. (1994). Motility voltage sensor of the outer hair cell resides within the lateral plasma membrane. *Proceedings of the National Academy of Sciences of the USA* **91**, 12268–12272.

Iwasa, K. H. (1993). Effect of stress on the membrane capacitance of the auditory outer hair cell. *Biophysical Journal* **65**, 492–498.

Iwasa, K. H. (1994). A membrane motor model for the fast motility of the OHC. *Journal of the Acoustical Society of America* **96**, 2216–2224.

Iwasa, K. H. & Adachi, M. (1997). Force generation in the outer hair cell of the cochlea. *Biophysical Journal* **73**, 546–555.

Kakehata, S. & Santos-Sacchi, J. (1995). Membrane tension directly shifts voltage dependence of outer hair cell motility and associated gating charge. *Biophysical Journal* **68**, 2190–2197.

Pusch, M. & Neher, E. (1988). Rates of diffusional exchange between small cells and a measuring patch pipette. *Pflügers Archiv* **411**, 204–211.

Ruggero, M. A. (1992). Responses to sound of the basilar membrane of the mammalian cochlea. *Current Opinion in Neurobiology* **2**, 449–456.

Santos-Sacchi, J. (1990). Fast outer hair cell motility: how fast is fast? In *The Mechanics and Biophysics of Hearing*, ed. Dallos, P., Geisler, C. D., Matthews, J. W., Ruggero, M. A. & Steele, C. R., pp. 69–75. Springer-Verlag, Berlin.

Santos-Sacchi, J. (1991). Reversible inhibition of voltage-dependent outer hair cell motility and capacitance. *Journal of Neuroscience* **11**, 3096–3110.

Santos-Sacchi, J. (1992). On the frequency limit and phase of outer hair cell motility: effects of the membrane filter. *Journal of Neuroscience* **12**, 1906–1916.

Santos-Sacchi, J. (1993). Harmonics of outer hair cell motility. *Biophysical Journal* **65**, 2217–2227.

Santos-Sacchi, J. & Dilger, J. P. (1988). Whole cell currents and mechanical responses of isolated outer hair cells. *Hearing Research* **35**, 143–150.

Santos-Sacchi, J., Huang, G.-J. & Kakehata, S. (1994). Variability of voltage dependency of the outer hair cell (OHC) motility voltage sensor. 127 th Meeting of the Acoustical Society of America, June.

Shepherd, G. M. & Corey, D. P. (1994). The extent of adaptation in bullfrog saccular hair cells. *Journal of Neuroscience* **14**, 6217–6229.

Skalak, R., Tozeren, A., Zarda, R. P., & Chein, S. (1973). Strain energy function of red blood cell membranes. *Biophysical Journal* **13**, 245–264.

Sridhar, T. S., Liberman, M. C., Brown, M. C. & Sewell, W. F. (1995). A novel cholinergic 'slow effect' of efferent stimulation on cochlear potentials in the guinea pig. *Journal of Neuroscience* **15**, 3667–3678.

Stefani, E., Toro, L., Perozo, E. & Bezanilla, F. (1994). Gating of Shaker K^+ channels: I. Ionic and gating currents. *Biophysical Journal* **66**, 996–1010.

Tolomeo, J. A. & Steele, C. R. (1995). Orthotropic piezoelectric properties of the cochlear outer hair cell wall. *Journal of the Acoustical Society of America* **97**, 3024–3029.

Tolomeo, J. A., Steele, C. R. & Holley, M. C. (1996). Mechanical properties of the lateral cortex of mammalian auditory outer hair cells. *Biophysical Journal* **71**, 421–429.

Tschoegl, N. W. (1989). *The Phenomenological Theory of Linear Viscoelastic Behavior*. Springer-Verlag, Berlin.

Acknowledgements

This work was supported by NIH-NIDCD grant DC00273 and DC02003 to J.S.S. We thank Margaret Mazzucco for technical help. We also thank Drs Robert Apfel, Hongbo Zhao and Francisco Bezanilla for helpful discussions.

Corresponding author

J. Santos-Sacchi: Surgery (Otolaryngology), BML 244, Yale University School of Medicine, 333 Cedar Street, New Haven, CT 06510, USA.

Email:joseph.santos-sacchi@yale.edu